scientific reports

Check for updates

OPEN

Sustainable uric acid sensor based on a lab-fabricated electrode modified with rice straw-derived carbon materials

Pakin Noppawan[1], Jaroon Jakmunee[2,3], Andrew J. Hunt[4], Nontipa Supanchaiyamat[4], Suwiwat Sangon[4], Jamras Lerdsri[5], Thidarat Kruatian[6] & Jantima Upan[1]✉

A novel and facile electrochemical sensor for the quantification of uric acid has been fabricated through the strategic modification of a screen-printed carbon electrode (SPCE) using mesoporous carbon-zinc oxide (MC-ZnO) synthesized from rice straw waste. The MC-ZnO materials, generated via a controlled pyrolysis process, exhibit homogeneous dispersion and a substantial electroactive surface area of 0.1286 cm^2. The electrochemical oxidation of uric acid exhibits a distinct peak at 0.18 V in differential pulse voltammetry (DPV), indicative of efficient charge transfer kinetics. A linear range spanning 20 to 225 µM was obtained with a limit of detection (LOD) of 3.76 µM, signifying exceptional analytical sensitivity. Furthermore, the sensor demonstrates robust selectivity toward uric acid in the presence of typical interferents, underscoring its applicability for precise uric acid determination in complex biological matrices. The sensor's analytical performance was validated by quantifying uric acid in spiked urine samples, yielding recovery rates between 97.9% and 114.8% and relative standard deviations (RSD) below 4.92%, affirming its accuracy and precision. This platform heralds a promising avenue for clinical diagnostics, leveraging sustainable materials for uric acid detection.

Keywords Agricultural waste, Biomass, Eco-friendly sensor, Modified electrode, Voltammetry

Currently, the measurement of uric acid has garnered significant interest due to its critical role in diagnosing and monitoring health conditions. Uric acid, a product of purine metabolism, is typically excreted via urine and blood[1]. The concentration of uric acid is approximately 1.19–2.98 mM per day in urine and ranges from 0.15 to 0.45 mM in the blood of healthy individuals[2]. Normally, healthy humans excrete between 400 and 700 mg of uric acid in their urine per day[3]. Elevated or reduced uric acid levels are associated with conditions such as gout, nephrolithiasis, and metabolic syndrome[4,5]. Therefore, the accurate, simple, and rapid determination of uric acid levels is crucial for effective medical diagnosis.

Multiple analytical approaches have been utilized to determine uric acid levels, including chromatographic methods[6,7], chemiluminescence[8], spectrophotometry[9,10], fluorimetry[11], and electroanalytical methods[12,13]. The enzymatic method is widely used due to its remarkable specificity and heightened sensitivity, involving the use of uric oxidase to catalyze the oxidation of uric acid, producing a measurable product. However, this method can be interfered with by other substances in the sample[14]. Spectrophotometry, while more cost-effective and simpler, generally offers lower specificity. In contrast, chromatographic methods provide high resolution but require sophisticated instrumentation and specialized expertise, making them often time-consuming and costly. Given these limitations, electrochemical sensors have emerged as a promising alternative because of their ability to overcome the drawbacks associated with traditional analytical methods. Data obtained from electroanalytical

[1]Department of Chemistry, Faculty of Science, Mahasarakham University, Maha Sarakham 44150, Thailand. [2]Research Laboratory for Analytical Instrument and Electrochemistry Innovation, Department of Chemistry, Faculty of Science, Chiang Mai University, Chiang Mai 50200, Thailand. [3]Research Laboratory on Advanced Materials for Sensor and Biosensor Innovation, Materials Science Research Center, Center of Excellence for Innovation in Chemistry, Faculty of Science, Chiang Mai University, Chiang Mai 50200, Thailand. [4]Materials Chemistry Research Center, Department of Chemistry, Center of Excellence for Innovation in Chemistry, Faculty of Science, Khon Kaen University, Khon Kaen 40002, Thailand. [5]Department of Livestock Development, Veterinary Research and Development Center (Upper Northern Region), Lampang 52190, Thailand. [6]Institute of Community Science Technology, Department of Science Service, Ministry of Higher Education, Science, Research and Innovation, Bangkok 10400, Thailand. ✉email: jantima.u@msu.ac.th

techniques provide valuable insights into electron transfer processes at the interfacial region and the associated electron transfer kinetics[15,16].

To minimize sensor size and chemical consumption, screen-printed electrodes (SPEs) are gaining notable interest due to their versatility, ease of customization and fabrication, flexibility, portability, reproducibility, and low cost[17]. The selection of the working electrode has a significantly influences on electrochemical sensor performance. Conventional working electrode often faces challenges such as surface fouling, retarded electron transfer reaction rates, and the impact of interfering chemical entities[18,19]. To address these challenges, carbon-based materials have been extensively employed for working electrode modification owing to their exceptional biocompatibility, negligible toxicity, and enhanced electrical conductivity[20,21]. Notably, the production of carbon materials derived from waste products aligns with the principles of green chemistry, promoting sustainable recycling and resource reuse[22].

In recent years, agricultural waste has become increasingly popular as a sustainable source of carbon-based materials[23–25]. Thailand's rice production and export volumes place it among the world's largest. In 2024, the Thai Rice Exporters Association reported that the country exported approximately 9.95 million tons of rice to various countries worldwide[26]. This statistic highlights the significant amount of agricultural waste, particularly rice straw, that is left behind. Given its abundance and low cost, rice straw presents a promising source of carbon materials. Additionally, it contains key components, for example, cellulose and lignin, which are versatile for the creation of high-performance, environmentally friendly carbon-based nanomaterials through chemical and thermal processes. Carbon materials derived from rice straw possess desirable properties, including high surface area, appropriate porosity, and electrical conductivity, making them particularly appropriate for the construction of electrochemical sensors[27]. Several investigations have indicated the potential of rice straw-based carbon materials in creating electrochemical sensors for the analysis of different analytes, including heavy metals, organic pollutants, and biomolecules[28–30]. These materials often exhibit excellent electrical conductivity, high surface area, and abundant pore structures, all of which are critical for enhancing the detection capabilities of electrochemical sensors by increasing sensitivity and selectivity. In a previous study, rice straw was employed as a precursor for the synthesis of highly mesoporous carbon-zinc oxide composites via pyrolysis, which to perform as highly effective photocatalytic adsorbents for toxic dye remediation[31]. The resulting composites exhibited a highly porous structure, large surface area, and homogeneous dispersion of the oxide phase, making them a promising modification for the electrode for uric acid analysis. To the best of our knowledge, sensors modified with rice straw-derived carbon materials have not been previously reported in the literature for the quantification of uric acid.

In this work, a screen-printed carbon electrode (SPCE) modified with eco-friendly carbonaceous materials derived from rice straw has been developed and investigated for uric acid determination for the first time. The formation of mesoporous carbon-zinc oxide composites (MC-ZnO) was achieved by pyrolysis. The parameters and validation characteristics of the method were investigated and optimized. The MC-ZnO-modified electrodes exhibited significantly enhanced electrochemical performance, characterized by superior conductivity, increased surface area, and improved catalytic activity toward uric acid oxidation reactions. The developed sensor successfully determined uric acid levels in urine samples, highlighting advantages such as low cost, ease of operation, and high sensitivity and selectivity.

Materials and methods

Chemicals and reagents

All chemicals were used without further purification. Deionized (DI) water (> 18 MΩ cm) was produced from a water purification system (Millipore, Sweden). Uric acid (> 99%) was purchased from Sigma-Aldrich, Hungary. Zinc chloride was from Ajax Finechem, Australia. Carbon ink was ordered from ACHESON, Singapore. Silver/silver chloride ink (Ag/AgCl) was received from Gwent Group of Companies, UK. Diethylene glycol monobutyl ether (98%) was obtained from Merck, Germany. A standard solution of uric acid was freshly prepared in 10 mM phosphate buffer, pH 7.0.

Materials and apparatus

The screen-printing block was obtained from Screen & Pad Printer Co., Ltd, Thailand. The polyvinyl chloride sheet with a thickness of 0.5 mm was purchased from China. The plasma cleaner used was the PDC-32G model from Harrick, USA. All electrochemical experiments were conducted using an Emstat potentiostat and the PStrace 5.8 program (PalmSens BV, Netherlands).

Preparation of lab-made spces

The lab-made SPCE was designed with three electrodes: a working electrode (WE) with an area of 7.07 mm^2, an auxiliary electrode (AE), and a reference electrode (RE). Carbon conductive ink was diluted with diethylene glycol monobutyl ether to achieve the desired viscosity. Next, the ink was screen-printed onto the surface of a flexible and thin polyvinyl chloride sheet, which acted as the substrate for the fabrication of WE and AE. Subsequently, the screen-printed ink was dried in an oven at 150 °C for 30 min. Following this, Ag/AgCl ink was applied to the channel of the RE and dried in an oven at 60 °C for 30 min. The fabricated SPCE was plasma-treated at 0.4 Torr under vacuum for 60 s to remove the residual polymer binder in the ink, expose a larger active area, and enhance the hydrophilic properties of the WE. The prepared SPCEs were kept at room temperature until use.

Preparation of carbon materials

MC-ZnO was synthesized from rice straw (RS) using zinc chloride ($ZnCl_2$) as an activator, following a previously reported procedure[31,32]. Briefly, rice straw was mixed with $ZnCl_2$ at biomass-to-activator ratios of 1:2, 1:3, and

2:3 (w/w) and allowed to stand for 24 h. The mixture was then dried at 110 °C for 5 h until a constant weight was achieved. Next, the dried material was activated at 500 °C and 700 °C under a nitrogen flow of 250 mL min^{-1} for 1 h. The resulting product was washed multiple times with deionized water until the wastewater reached a neutral pH. Finally, the composite was dried at 110 °C to remove residual moisture and labeled as RS-2$ZnCl_2$-500, RS-2$ZnCl_2$-700, RS-3$ZnCl_2$-700, and 2RS-3$ZnCl_2$-700.

Preparation of the modified SPCE

Before modifying the electrode, the MC-ZnO suspension was prepared. The carbon powder was finely ground using a mortar. Next, 2 mg of the material was dispersed in 1 mL of ethanol and sonicated at room temperature for 60 min to achieve a homogeneous suspension. Afterward, 2.0 µL of the suspension with a concentration of 2 mg mL^{-1} was carefully dropped to the surface of the WE of the lab-made SPCE and dried at ambient temperature.

Electrochemical determination of uric acid

The electrochemical oxidation of uric acid was investigated using differential pulse voltammetry (DPV). The electrochemical cell consisted of the MC-ZnO/SPCE as WE, carbon as AE, and Ag/AgCl as RE, with 10 mM phosphate buffer at pH 7.0 as a supporting electrolyte. To perform the analysis, the electrode was immersed in a 10-mL beaker containing 5.0 mL of uric acid solution. The DPV experiments were conducted by applying a potential range from −0.40 V to 0.80 V, with a step potential of 0.025 V and a scan rate of 0.075 V s^{-1}. All experiments were conducted in triplicate. A schematic illustration of the sensor preparation and detection process is presented in Fig. 1.

Results and discussion

Investigation of various electrode materials derived from rice straw for modifying SPCE

This research investigates the advancement of the sophisticated electrochemical method for uric acid quantification. To achieve this, SPCEs are modified with carbonaceous materials derived from rice straw, a readily available and sustainable agricultural byproduct. The carbon materials are synthesized by pyrolysis under controlled conditions. Several straw-based carbon-zinc oxide materials, employing $ZnCl_2$ as a template, are fabricated. Each electrode material is subsequently utilized to coat the working electrode. The electrochemically accessible surface area (EASA) of the modified working electrode of SPCE is assessed using cyclic voltammetry (CV) analytical determinations within a solution containing 10 mM ferri-ferro cyanide. The EASAs are calculated by the Randles-Sevcik Eqs[33,34], which can be expressed as:

$$\mathrm{Ip} = 2.69 \times 10^5 \mathrm{n}^{3/2} \mathrm{AD}^{1/2} \mathrm{Cv}^{1/2}$$

The calculated effective EASA values of the bare SPCE, RS-2$ZnCl_2$-500/SPCE, RS-2$ZnCl_2$-700/SPCE, RS-3$ZnCl_2$-700/SPCE, and 2RS-$ZnCl_2$-700/SPCE are determined to be 0.1194 cm^2, 0.1286 cm^2, 0.1353 cm^2, 0.1622 cm^2, and 0.0945 cm^2, respectively. These results highlight that the EASA is significantly influenced by both the $ZnCl_2$ ratio and the activation temperature during the synthesis process. The variation in EASA plays a critical role in these parameters in optimizing the electrode's surface properties for enhanced electrochemical performance.

Furthermore, a comparative investigation has been performed to evaluate the oxidative response of uric acid at a concentration of 1.0 mM in phosphate buffer at pH 7.0 using various modified SPCEs. This study intends to determine the performance characteristics of each modified electrode in terms of sensitivity and

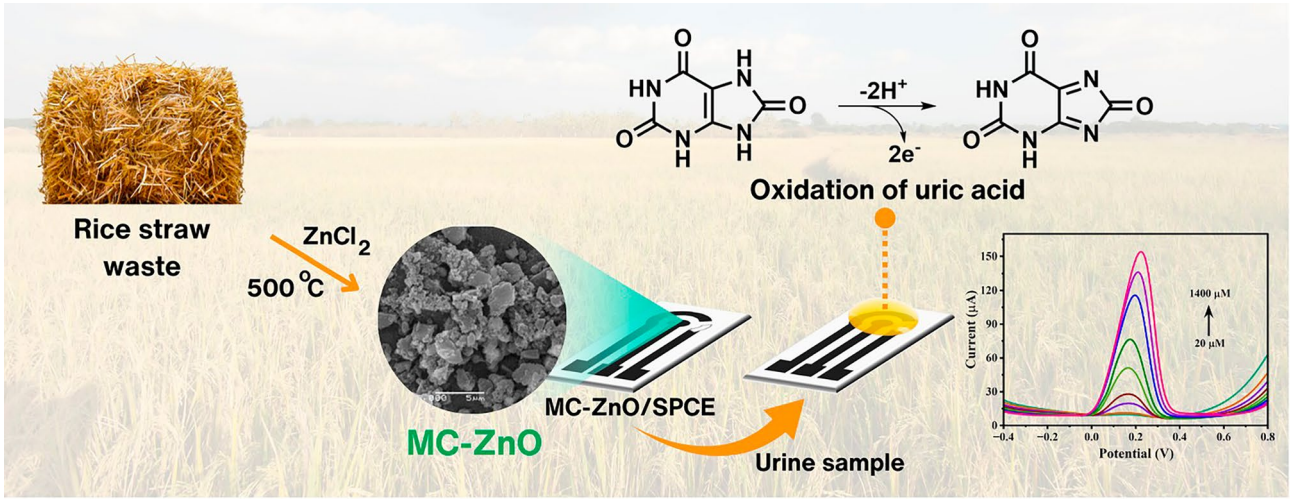

Fig. 1. Schematic representation of the fabrication and working principle of the electrochemical sensor for uric acid detection.

overall electrochemical activity, providing valuable insights into the effect of surface modifications on the determination of uric acid under physiological pH conditions. The results, as summarized in Table 1, reveal that the RS-2$ZnCl_2$-500/SPCE exhibits the highest current response for uric acid oxidation among all tested electrodes. This improved performance is due to the optimized surface properties of the RS-2$ZnCl_2$-500/SPCE, which may result from a synergistic balance between the $ZnCl_2$ ratio and the activation temperature during its synthesis. The findings emphasize the critical influence of surface modification strategies on improving electrode sensitivity and catalytic activity, revealing important principles for the formulation of innovative materials in electrochemical sensing. Consequently, RS-2$ZnCl_2$-500/SPCE is selected for further experiments.

Surface morphologies and properties of the RS-2$ZnCl_2$-500

The RS-2$ZnCl_2$ material was successfully characterized in a previous study[32]. Advanced imaging techniques, including transmission electron microscopy (TEM) and scanning electron microscopy (SEM), are utilized to thoroughly examine its surface morphology. TEM provides high-resolution insights into the internal structure of the material, revealing critical details such as particle size, shape, and distribution. Meanwhile, SEM offers complementary information on its surface topography and textural properties. These comprehensive analyses confirm the structural integrity, uniformity, and high-quality synthesis of the RS-2$ZnCl_2$ material. Furthermore, prior results identify RS-2$ZnCl_2$ as one of the mesoporous carbon-zinc oxide (MC-ZnO) composites, further demonstrating its potential for advanced electrochemical applications.

Nitrogen adsorption–desorption analysis was used to investigate the pore structure of the activated carbons, and the adsorption–desorption isotherms are shown in Fig. S1. The activated carbon sample 2RS-$ZnCl_2$-700 displayed a mixture of type I and type IV isotherms, with a small hysteresis loop, indicating an extensively microporous structure[35]. In contrast, carbons with higher $ZnCl_2$/RS ratios exhibited type IV isotherms with a hysteresis loop, suggesting significant mesoporosity[36]. The pyrolyzed rice straw with $ZnCl_2$ activation showed surface areas ranging from 418 to 1001 m^2/g. The RS-2$ZnCl_2$-500 sample exhibited the highest surface area of 1001.0 m^2/g, followed by RS-2$ZnCl_2$-700 (833.1 m^2/g), RS-3$ZnCl_2$-700 (709.5 m^2/g), and 2RS-$ZnCl_2$-700 (418.3 m^2/g) as summarized in Table S1. Lower $ZnCl_2$ impregnation resulted in less dehydration and pore formation, whereas higher $ZnCl_2$ ratios led to significant dehydration, promoting pore widening, which reduced the surface area and microporosity[31]. $ZnCl_2$ also prevents tar accumulation on the surface, enhancing decomposition and porosity development[37].

Powder X-ray diffraction (XRD) analysis revealed that the activated carbons obtained via $ZnCl_2$ activation exhibited sharp peaks at 31.63°, 34.18°, 38.94°, 49.06°, 65.80°, 68.86°, and 70.30°, which correspond to the 001, 002, 101, 102, 200, 112, and 201 planes of the hexagonal wurtzite structure of ZnO, respectively. This indicates the presence of ZnO within the carbon structure (Fig. 2), in good agreement with values reported in the literature[38]. Additionally, peaks at 22.25° and 25.73°, corresponding to SiO_2, were also observed[39]. Interestingly, the XRD pattern of RS-2$ZnCl_2$-500 did not show sharp peaks associated with ZnO crystallinity but instead displayed features characteristic of a graphitic structure in the carbon material around 28° and 36°.

X-ray photoelectron spectroscopy (XPS) was performed to examine the chemical state of Zn. The XPS spectra confirmed the presence of ZnO in the RS-2$ZnCl_2$-500 sample. The peaks at around 1023 eV and 1046 eV correspond to the Zn $2p_3/_2$ and Zn $2p_1/_2$ levels, respectively (Fig. S2)[40]. The peak at 1020–1022 eV was attributed to ZnO, while the peaks at 1023–1025 eV were assigned to $Zn(OH)_2$, with both components expected in ZnO[41]. In the O 1s region, five peaks were observed at 531, 532, 533, 534, and 536 eV, corresponding to oxygen in the ZnO crystal lattice (OL). The peaks at 531 and 532 eV were assigned to zinc oxide and hydroxy oxygen (OOH), respectively, while the peak at 533 eV was attributed to chemisorbed oxygen, possibly from molecular water or carboxylate- or carbonate-type species[42]. In the C 1s region, the main peak observed at 285 eV was assigned to hydrocarbon species. Smaller peaks at 286 eV, 287 eV, and 289 eV were attributed to C–O bonds, carbonyl/carboxyl, and/or carbonate species[43]. Notably, a feature around 284–283 eV, assigned to graphitic carbon, was observed in RS-2$ZnCl_2$-500, confirming the presence of a graphitic structure within the material[44].

Herein, a SEM is utilized to investigate the native exterior morphology. The bare SPCE exhibits a relatively smooth and large surface with visible graphite sheets, as shown in Fig. 3a, which are characteristic of the carbon ink. The MC-ZnO-modified SPCE demonstrates a distribution of numerous particles and a notable increase in exterior roughness as presented in Fig. 3b, consequently providing a larger effective working area. These findings indicate that MC-ZnO is effectively applied to the SPCE surface, confirming the successful fabrication of the MC-ZnO/SPCE working electrode. Moreover, the particle size distribution, determined from the SEM images in Fig. 3b, revealed that the MC-ZnO particles range in size from 1.0 to 4.5 µm, with an average particle size of 2.3 µm. EDS examination reveals its composition to be approximately 94.2% carbon, 5.7% oxygen, and 0.1% chlorine (Fig. 3c). In contrast, the MC-ZnO/SPCE shows a significant shift in elemental composition. EDS

Electrode materials	Current (µA) obtained from 10 mM ferri-ferrocyanide	Electrochemical active surface area (cm^2)	Current (µA) obtained from 0.1 mM uric acid
Bare SPCE	178.5	0.1194	20.3
RS-2$ZnCl_2$-500/SPCE	192.2	0.1286	28.0
RS-2$ZnCl_2$-700/SPCE	202.0	0.1353	21.5
RS-3$ZnCl_2$-700/SPCE	242.5	0.1622	16.0
2RS-$ZnCl_2$-700/SPCE	141.3	0.0945	20.3

Table 1. Electrochemical active surface area and performance of electrode materials applied for uric acid quantification.

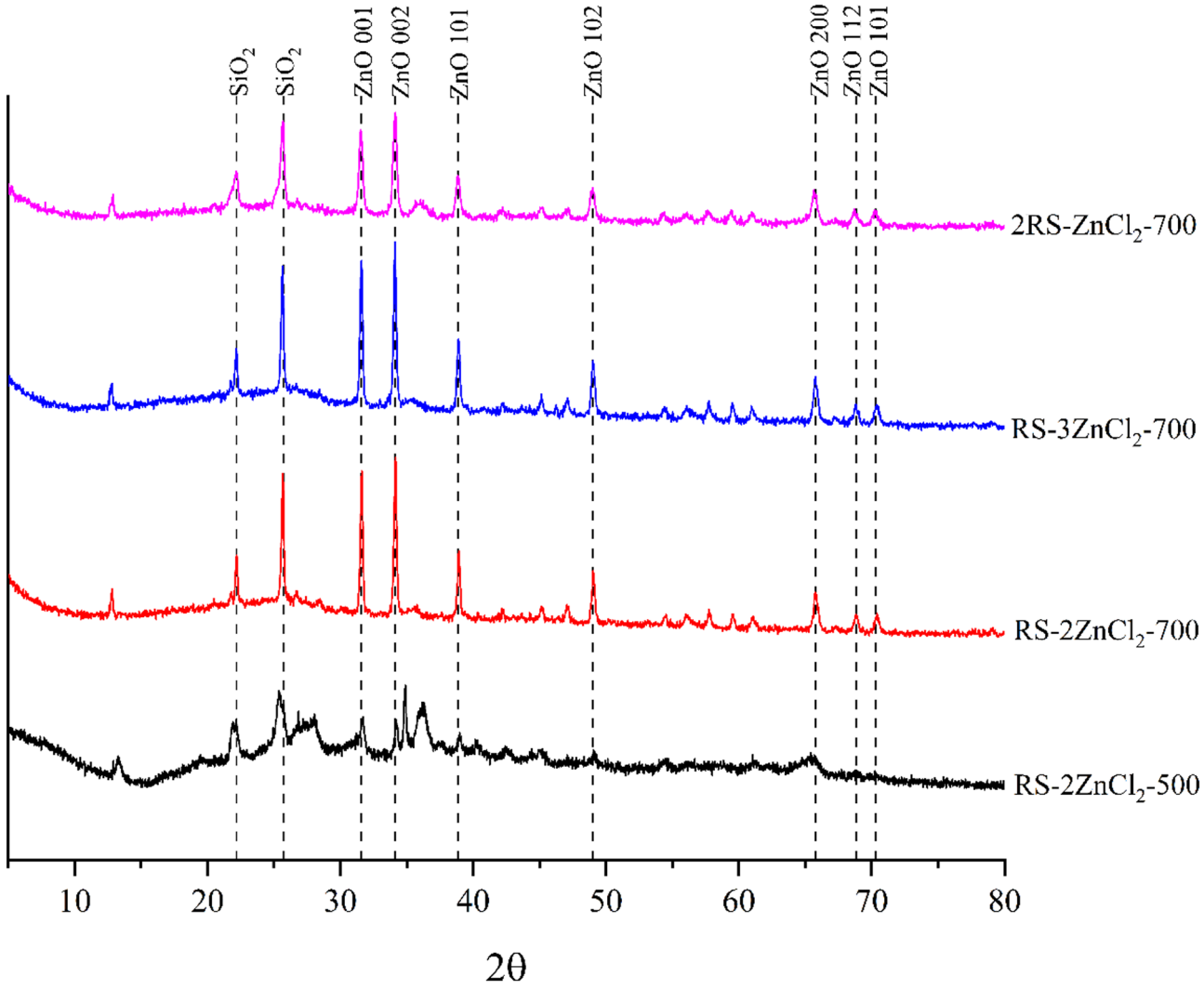

Fig. 2. XRD patterns of $ZnCl_2$-activated carbons.

analysis indicates a decrease in carbon to 79.3% while introducing additional elements: 14.0% oxygen, 3.3% zinc, 1.8% iron, 1.2% calcium, 1.5% magnesium, and 0.2% silicon (Fig. 3d). This elemental change confirms the successful modification of the SPCE surface with MC-ZnO. Further characterization by TEM reveals that the MC-ZnO material exhibits a heterogeneous structural distribution, characterized by a granular and rough morphology as shown in Fig. 2e, which consequently results in a larger effective exterior area. Additionally, the distinct material structure and surface morphology, as observed in SEM and EDS analysis, further substantiate the completed production and adjustment of the electrode's exterior.

Suitable amount of MC-ZnO for modifying the working electrode

To optimize the performance of the uric acid sensor, the appropriate quantity of MC-ZnO for electrode modification is systematically evaluated. DPV analysis reveals that 15 µL of the MC-ZnO suspension is the optimal amount for modifying the SPCE surface, yielding the highest current response as shown in Fig. S3. Conversely, using quantities exceeding this threshold results in a slight decrease in current, likely due to the agglomeration of carbon particles, which reduces the effective surface area available for electrochemical interactions. On the other hand, quantities below 15 µL provided insufficient carbon material, thereby limiting the interaction between the electrode surface and uric acid molecules. Consequently, 15 µL is identified as the optimal quantity for subsequent electrode modification procedures. The modified electrodes demonstrate markedly enhanced electrochemical performance, including superior conductivity, an expanded surface area, and heightened catalytic efficacy toward uric acid oxidation reactions.

Electrochemical characterization of the MC-ZnO/SPCE

The electrochemical properties of the modified SPCE were compared to those of the unmodified SPCE using CV and electrochemical impedance spectroscopy (EIS) in 10 mM ferri-ferrocyanide solution. Well-defined anodic and cathodic peaks were observed for both electrodes, as shown in Fig. 4a. However, the MC-ZnO/

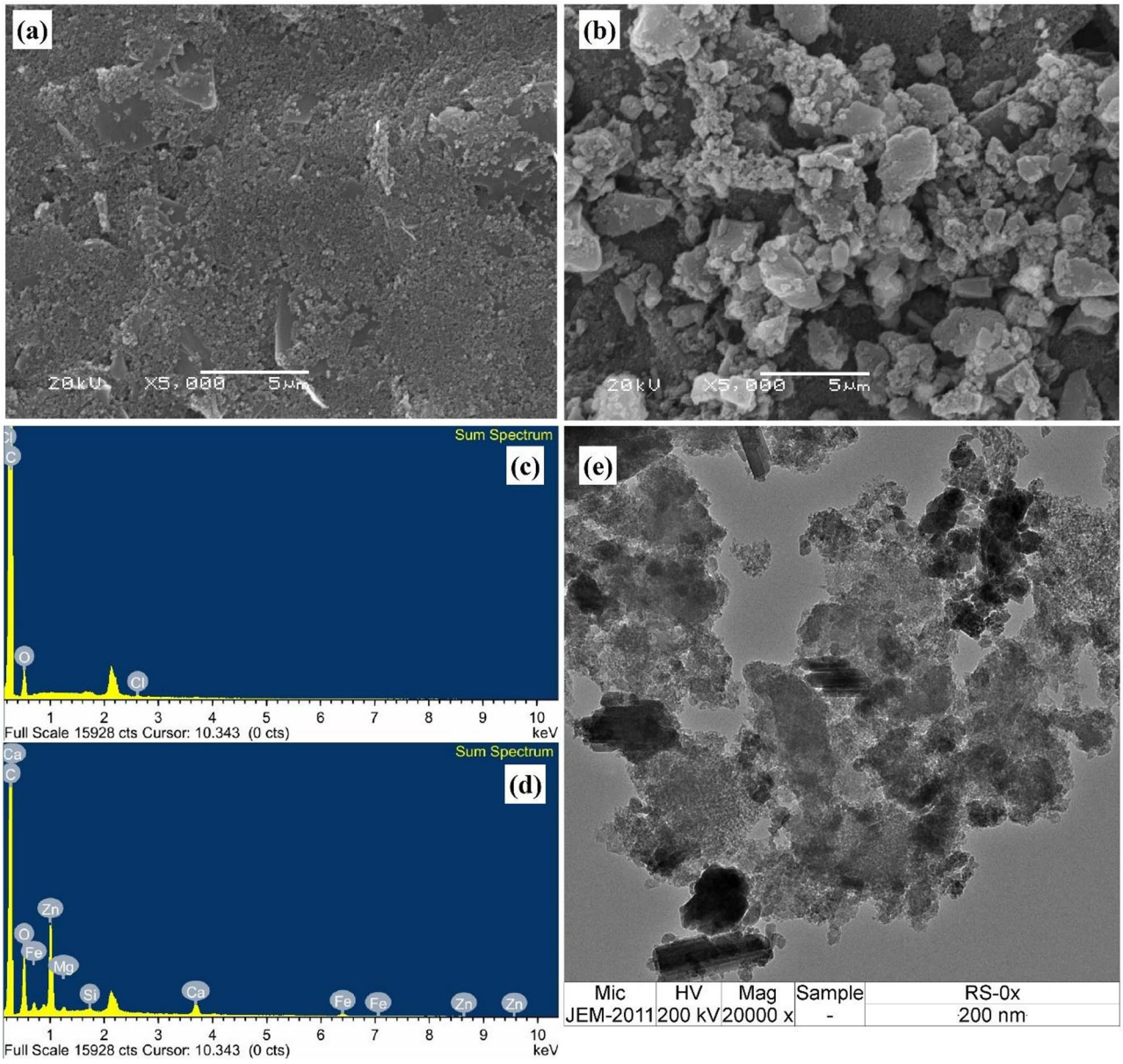

Fig. 3. SEM images of bare SPCE (**a**) and MC-ZnO/SPCE (**b**), EDS spectra of bare SPCE (**c**) and MC-ZnO/SPCE (**d**), and TEM image of MC-ZnO (**e**).

SPCE exhibited a higher current response than the bare SPCE, indicating a large electroactive surface area and high electrical conductivity of the MC-ZnO material, which enhances the electron transfer rate at the electrode interface. Furthermore, the EIS results were consistent with the CV findings. The Nyquist plot of the MC-ZnO/SPCE displayed a smaller semicircle than that of the bare SPCE, as presented in Fig. 4b, indicating reduced electron transfer resistance. This reduction is attributed to the improved conductivity and more efficient electron transport pathways provided by the MC-ZnO composite. These findings highlight the potential of MC-ZnO-modified SPCE as a promising platform for the development of electrochemical sensor.

Electrochemical process of uric acid on the MC-ZnO/SPCE

The phosphate buffer solution's pH significantly influences the electrochemical reaction. As the buffer's alkalinity increases, the uric acid electrochemical reaction's potential shifts towards less positive values, as illustrated in Fig. 5a. A significant association between $E_{p.a.}$ and pH values is evident in Fig. 5b, as described by the linear equation: $E_{p.a.}$ (V) = – 0.057pH + 0.643 (r^2 = 0.9923). A slope of – 0.057 V/pH indicates that the uric acid oxidation mechanism entails a transfer of an equal count of electrons and protons. This near-Nernstian characteristic suggests a stable electrochemical reaction, most probably mediated by a two-electron, two-proton transfer process within the established experimental parameters[45]. The relationship between potential and pH further highlights the significant influence of the proton concentration regarding the electrochemical response of uric acid, underscoring the importance of maintaining precise pH control in such analyses. Furthermore, the optimal

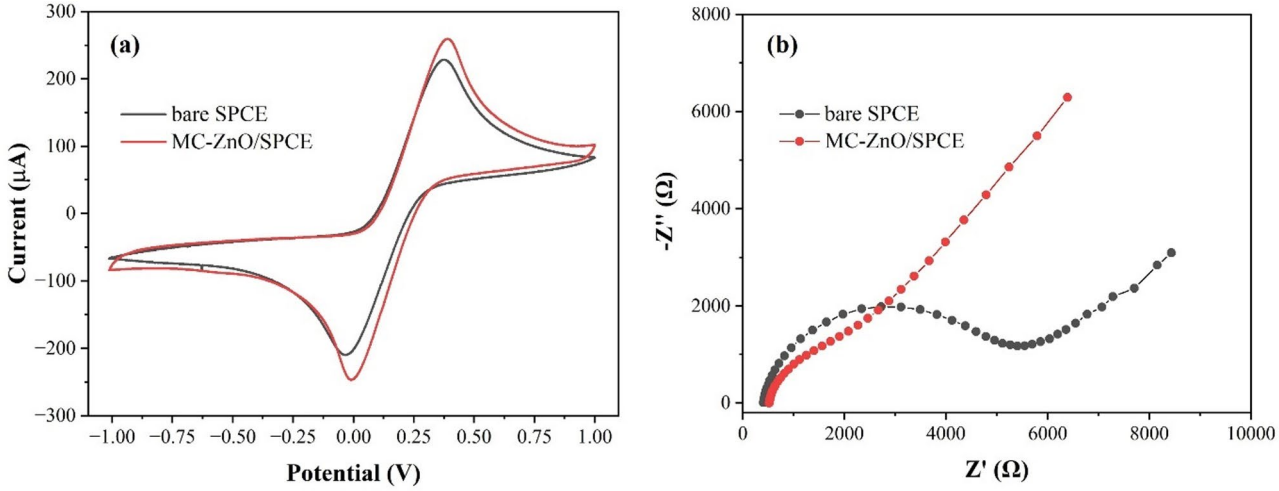

Fig. 4. Cyclic voltammograms (**a**) and Nyquist plots (**b**) of bare SPCE and MC-ZnO/SPCE in 10 mM ferri-ferrocyanide.

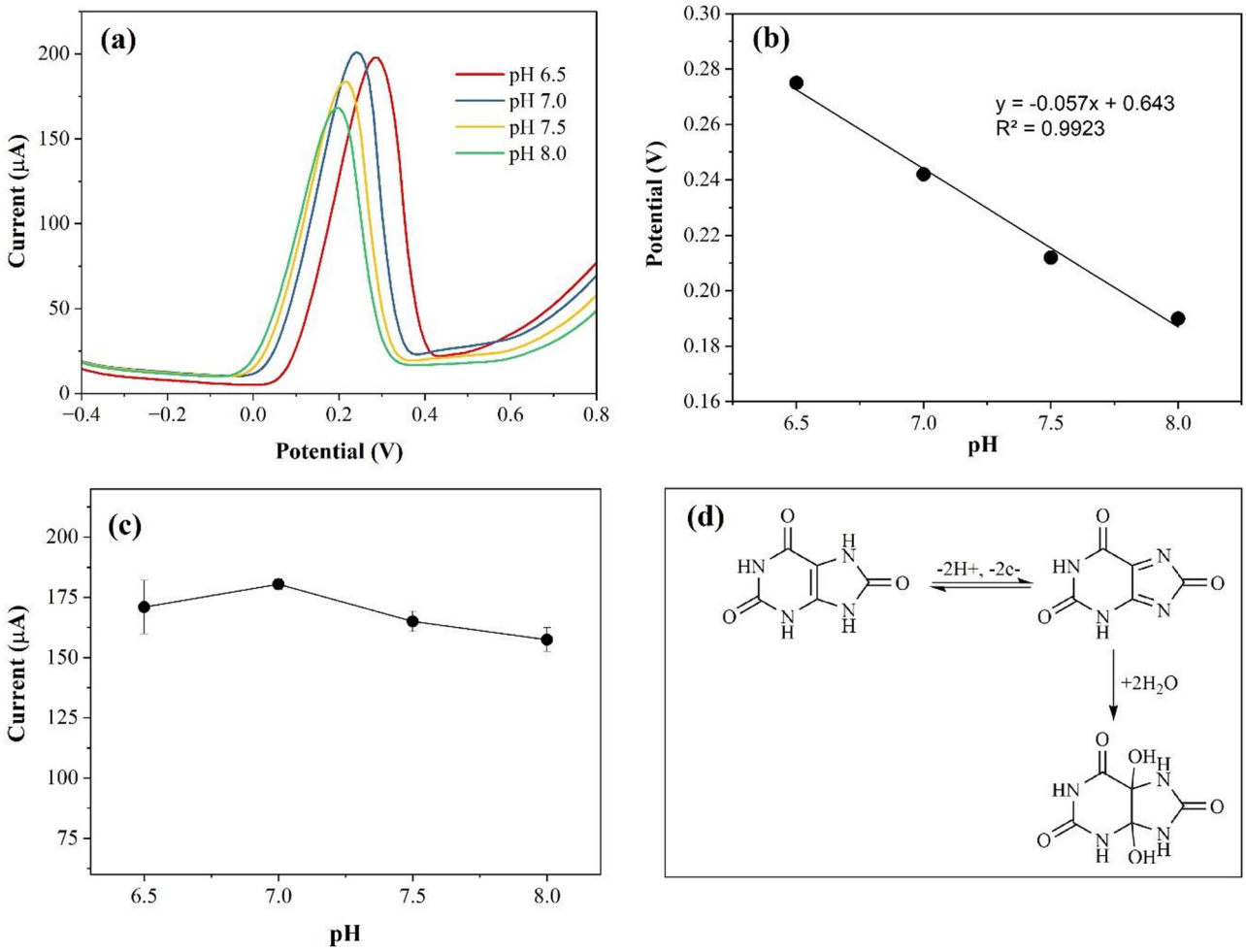

Fig. 5. The pH optimization for uric acid detection using MC-ZnO/SPCE consisted of DPV peaks of 0.1 mM uric acid in phosphate buffer solutions across a range of pH values (**a**), oxidation potential as a function of pH (**b**), anodic peak current and phosphate buffer pH (**c**), and proposing an electrochemical mechanism for uric acid oxidation and product formation (**d**).

pH range for analysis from 6.5 to 8.0 is explored. The DPV response of uric acid on the MC-ZnO/SPCE is recorded, as illustrated in Fig. 5c. A decline in oxidative current magnitudes is observed at pH values both above and below 7.0. These findings suggest that the specific buffer at pH 7.0 yields the highest current response, making it the optimal condition for the analysis. The proposed electrochemical mechanism of uric acid oxidation and its reaction product are illustrated in Fig. 5d. Briefly, when an appropriate potential is applied to the modified SPCE, uric acid molecules undergo oxidation at the electrode surface. During this process, electrons are transferred, generating a current response that is directly proportional to the uric acid concentration.

Effect of scan rate

The application of CV has been utilized to determine whether the electrochemical process of uric acid is diffusion-controlled, where measurement proceeds without the necessity of uric acid accumulation taking place on the electrode's exterior, or regulated by adsorption interactions, which require prior accumulation. Figure 6a depicts the electrochemical behavior of uric acid on MC-ZnO/SPCE analyzed via CV measurement. As the potential scan rate increased, a progressive rise in oxidation currents was observed. A linear correlation exists between the oxidation current and the square root of the scan rate, with a correlation coefficient (r^2) of 0.9927 as presented in Fig. 6b. This result unequivocally indicates that the electrochemical oxidation of uric acid on MC-ZnO/SPCE appears to be diffusion-controlled, mirroring the behavior seen on conventional glassy carbon electrode[45]. In this diffusion-controlled mechanism, rapid electron transfer facilitates the efficient diffusion of uric acid from the migration of solute from the bulk solution to a region of lower concentration at the electrode's exterior. This diffusion-dependent process offers the advantage of faster measurement times compared to adsorption-controlled mechanisms. As a result, it eliminates the need for a time-consuming enrichment step on the electrode surface, significantly improving detection efficiency.

Optimization of DPV parameters

Some important parameters for the DPV measurement, which influence the anodic peak current of uric acid, are optimized to achieve a higher sensitivity. Step potential is a parameter that refers to the potential increment applied between each pulse during the measurement. It can affect the resolution and sensitivity of the voltammogram. The step potential is studied within a range of 0.005 to 0.100 V. The current increases with the step potential up to 0.025 V, after which it slightly decreases. Additionally, applying a higher step potential results in lower signal resolution, causing the voltammograms to be less defined. Therefore, a step potential of 0.025 V is chosen as the optimal condition. Since the potential scan velocity influences the magnitude of the current intensity, the effect of potential scan velocity is investigated in the range of 0.05 to 0.20 V s^{-1}. At higher scan rates, the current increases due to the faster electrochemical reaction, which allows for greater charge transfer within a shorter time. However, high scan rates lead to less defined peaks. To obtain well-defined peaks and a high current, a potential scan velocity of 0.075 V s^{-1} is selected for further experiments.

Range and linearity

Figure 7a illustrates the DPV response of uric acid measured at the MC-ZnO/SPCE under the optimal conditions. The developed sensor exhibits excellent electron-mediating properties, as demonstrated by a distinct oxidation peak at approximately 0.18 V, corresponding to the electrochemical oxidation of uric acid. As the concentration of uric acid increases, a corresponding enhancement of the oxidation current is observed, highlighting the sensor's ability to detect varying amounts of uric acid with high sensitivity. The relationship between the dependence of electrochemical oxidation on uric acid amounts is depicted in Fig. 7b. A linear correlation has been established within the amount range of 20–225 µM, with a coefficient of determination (r^2) of 0.9997, demonstrating exceptional reliability of the sensor for uric acid quantification. A limit of detection

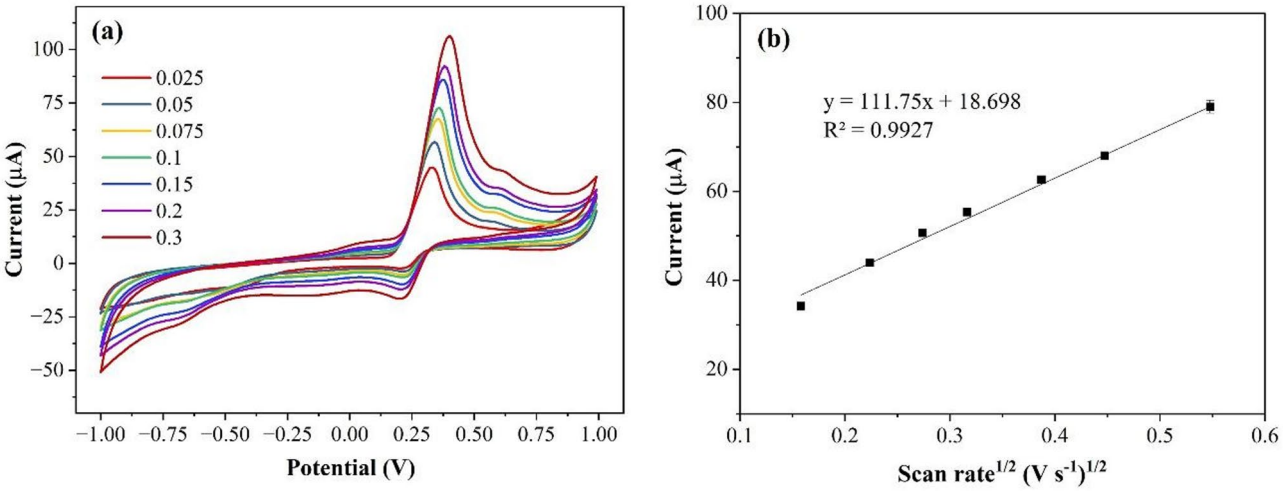

Fig. 6. Cyclic voltammograms of 0.1 mM uric acid in phosphate buffer (pH 7.0) recorded at varying scan rates (**a**) and Linear correlation between the oxidation current and the square root of the scan rate (**b**).

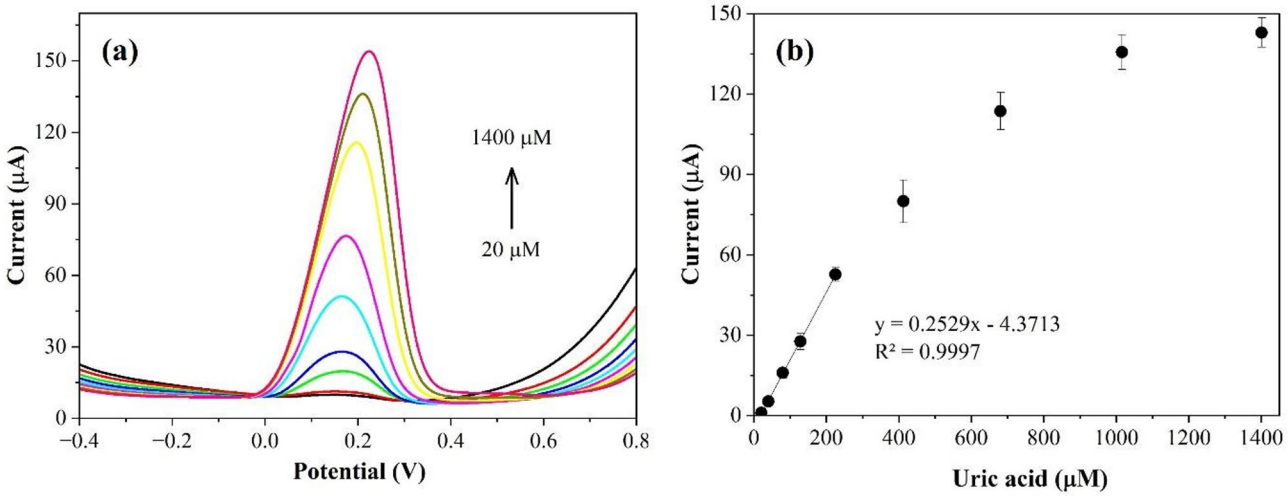

Fig. 7. DPV peaks of varying uric acid concentrations (**a**) and Linear calibration plot for the determination of uric acid (**b**).

Modifications	Electrode	Linear range (µM)	LOD (µM)	References
Fe_3O_4	GCE	20–160	14	[46]
Co_3O_4 porous NSs	GCE	0–800	12	[47]
ZnO/PANI	CPE	10–120	7	[48]
ZIF-8/rGO	SPCE	20–400	0.97	[49]
N, S-CAB-CNTs	SPCE	0.8–100, 200–1000	0.49	[50]
$Ni(OH)_2$-NiO(OH)/PANI-CNTs	SPCE	5–800	0.11	[51]
MC-ZnO	Lab-made SPCE	20–225	3.76	This work

Table 2. The performances of different materials modified electrodes for the determination of uric acid. *GCE* glassy carbon electrode, *Fe_3O_4* iron oxide nanoparticles, *Co_3O_4porous NSs* porous cobalt oxide nanosheets, *PANI* polyaniline, *CPE* carbon paste electrode, *ZIF-8* zeolitic imidazolate framework-8, *rGO* reduced graphene oxide, *N, S-CAB-CNTs* nitrogen and sulfur co-doped activated conductive acetylene black and carbon nanotubes, *CNTs* carbon nanotubes.

(LOD) has been successfully determined based on the 3SD/slope method and found to be 3.76 µM. The analytical performance of the developed MC-ZnO/SPCE sensor, utilizing simple, environmentally friendly, and cost-effective materials, is comparable to that of other sensors reported in the literature as shown in Table 2. The high degree of linearity and low LOD confirms its potential for quantitative analysis, making it a valuable tool for sensitive and accurate quantification of uric acid in a range of biological and clinical applications.

Selectivity

The results of the selectivity evaluation of the developed sensor are presented in Fig. S4. The findings demonstrate that the method exhibits excellent specificity towards uric acid, with minimal interference from common compounds, including glucose, sucrose, ascorbic acid, dopamine, melatonin, epinephrine, sodium ions, potassium ions, and chloride ions. This sensor highlights the robustness and reliability for uric acid determination in complex matrices. However, dopamine significantly interferes with the quantification of uric acid, because dopamine has a high tolerance threshold of 100 µM due to its susceptibility to electrochemical oxidation, which overlaps with the uric acid oxidation signal[52].

Furthermore, specific components present in urine samples may interact on the MC-ZnO surface, obstructing the diffusion of uric acid within the specific media and hindering electron transfer throughout the uric acid oxidation process. To mitigate the effects of these interfering substances, a standard addition method is employed for uric acid quantification.

Reproducibility and stability of the MC-ZnO/SPCE

Five sensors (MC-ZnO/SPCEs) were fabricated utilizing the same procedure. These electrodes are thereafter implemented to determine uric acid. The results in Fig. S5(a) exhibit remarkable intra-electrode precise measurements, yielding a relative standard deviation (RSD) of 6.82%. To assess the stability of the fabricated MC-ZnO/SPCEs, they are subjected to refrigerated storage at 4 °C in a sealed container for varying durations. Subsequently, their electrochemical performance has been evaluated by measuring the current response towards

Sample and spiked concentration	Analytical performance		
	Found (μM)	Recovery (%)	RSD (%)
Urine 1	21.16	–	2.96
Spiked concentration, 30 μM	52.92	105.9	3.50
Spiked concentration, 60 μM	83.01	103.1	1.91
Urine 2	25.75	–	2.49
Spiked concentration, 30 μM	55.14	98.0	4.84
Spiked concentration, 60 μM	87.77	103.4	0.45
Urine 3	23.37	–	4.79
Spiked concentration, 30 μM	55.06	105.6	0.38
Spiked concentration, 60 μM	87.12	106.3	4.92

Table 3. Analytical performance of the developed DPV method utilizing MC-ZnO/SPCE for determining uric acid in urine samples.

the same analyte concentration. The working electrodes exhibit reduced stability, showing a gradual decline in current response compared to the initial measurement. A deterioration of approximately 50% in current response is observed after two weeks of storage as shown in Fig. S5(b). This decrease is likely due to the MC materials' tendency to adsorb moisture and gases, which reduces the effective electrode surface area. Therefore, storage conditions should be further investigated to enhance the sensor's stability. In the meantime, the preparation of fresh electrodes is recommended to ensure consistent and reliable analytical performance.

Quantification of uric acid in urine samples

The MC-ZnO/SPCE working electrode, in conjunction with the DPV technique, has been utilized to quantify uric acid concentrations in three urine samples, thereby evaluating the applicability of the presented method employing the standard addition procedure. The accuracy and precision of the sensor are evaluated at two levels (30 and 60 μM) for each sample. The determined uric acid concentrations in the urine samples are 21.16, 25.75, and 23.37 μM, respectively. The mean recoveries for fortified urine samples range from 98.0 to 106.3%, with acceptable %RSD values below 5%. These findings confirm that the MC-ZnO/SPCE based on the DPV method provides highly accurate and precise measurements of uric acid, as summarized in Table 3. The method satisfies the required validation parameters, demonstrating its reliability for uric acid quantification in biological matrices.

Conclusions

This research has successfully engineered a novel and innovative electrochemical analytical device for uric acid detection by modifying screen-printed carbon electrodes with MC-ZnO composites derived from the sustainable and abundant agricultural byproduct, rice straw. This innovative approach not only enhances the environmental sustainability of the sensor but also leverages the unique properties of ZnO to significantly improve its performance. The optimized sensor exhibits exceptional analytical characteristics, demonstrating high sensitivity and selectivity towards uric acid in a matrix simulating the presence of interfering substances found in urine. This high selectivity is crucial for ensuring the accurate and reliable quantification of uric acid in complex matrices such as urine. Furthermore, the MC-ZnO modification significantly enhances the electrode's electrochemical properties by increasing its conductivity, surface area, and catalytic activity towards uric acid oxidation. The sensor's practical applicability has been further validated through accurate and precise uric acid quantification in biological urine matrices. This innovative approach not only offers a promising alternative to conventional analytical methods but also highlights the potential of utilizing sustainable and eco-friendly materials in the development of advanced electrochemical detection.

Data availability

The data supporting the research findings can be obtained from the corresponding author, upon reasonable request.

Received: 22 March 2025; Accepted: 20 May 2025
Published online: 26 May 2025

References

1. Svistounov, D. et al. Development of quantitative assay for simultaneous measurement of purine metabolites and creatinine in biobanked urine by liquid chromatography-tandem mass spectrometry. *Scand. J. Clin. Lab. Invest.* **82** (1), 37–49. https://doi.org/10.1080/00365513.2021.2015799 (2022).
2. Khan, M. I. et al. Portable electrophoresis Titration chip model for sensing of uric acid in urine and blood by moving reaction boundary. *Sens. Actuators B.* **286**, 9–15. https://doi.org/10.1016/j.snb.2019.01.098 (2019).
3. Chenthattil, R. et al. Validated electrochemical method for simultaneous resolution of tyrosine, uric acid, and ascorbic acid at polymer modified nano-composite paste electrode. *Surf. Eng. Appl. Electrochem.* **56** (4), 415–426. https://doi.org/10.3103/s1068375520040134 (2020).
4. Richette, P. & Bardin, T. Gout. *Lancet* **375** (9711), 318–328. https://doi.org/10.1016/S0140-6736(09)60883-7 (2010).

5. Zhao, C., Jiao, Y., Hu, F. & &Yang, Y. Green synthesis of carbon Dots from pork and application as nanosensors for uric acid detection. *Spectrochim Acta Mol. Biomol. Spectrosc.* **190**, 360–367. https://doi.org/10.1016/j.saa.2017.09.037 (2018).
6. Mohammed, O. J., Saeed, A. M. & Mohammed, I. S. RP-HPLC developed method for uric acid Estimation in human serum. *Res. J. Pharm. Technol.* **12**, 4703–4708. https://doi.org/10.5958/0974-360X.2019.00810.2 (2019).
7. Sun, Y. P., Chen, J., Qi, H. Y. & Shi, Y. P. Graphitic carbon nitrides modified Hollow fiber solid phase Microextraction for extraction and determination of uric acid in urine and serum coupled with gas chromatography-mass spectrometry. *J. Chromatogr. B Anal. Technol. Biomed. Life Sci.* **1004**, 53–59. https://doi.org/10.1016/j.jchromb.2015.09.025 (2015).
8. Shi, B., Su, Y., Duan, Y., Chen, S. & Zuo, W. A nanocomposite prepared from copper (II) and nitrogen-doped graphene quantum Dots with peroxidase mimicking properties for chemiluminescent determination of uric acid. *Microchim Acta*. **186**, 397. https://doi.org/10.1007/s00604-019-3491-9 (2019).
9. Wang, X. et al. A highly selective and sensitive colorimetric detection of uric acid in human serum based on MoS_2-catalyzed oxidation TMB. *Anal. Bioanal Chem.* **411**, 943–952. https://doi.org/10.1007/s00216-018-1524-6 (2019).
10. Liang, C. et al. Synthesis of carbon quantum Dots with iron and nitrogen from Passiflora edulis and their peroxidase-mimicking activity for colorimetric determination of uric acid. *Microchim Acta*. **187** (7), 405. https://doi.org/10.1007/s00604-020-04391-8 (2020).
11. Jin, D. et al. Quantitative determination of uric acid using CdTe nanoparticles as fluorescence probes. *Biosens. Bioelectron.* **77**, 359–365. https://doi.org/10.1016/j.bios.2015.09.057 (2016).
12. Sriram, B. et al. Novel sonochemical synthesis of Fe_3O_4 nanospheres decorated on highly active reduced graphene oxide nanosheets for sensitive detection of uric acid in biological samples. *Ultrason. Sonochem.* **58**, 104618. https://doi.org/10.1016/j.ultsonch.2019.104618 (2019).
13. Baccarin, M., Rowley-Neale, S. J., Cavalheiro, E. T. G., Smith, G. C. & Banks, C. E. Nanodiamond based surface modified screen-printed electrodes for the simultaneous voltammetric determination of dopamine and uric acid. *Microchim Acta*. **186**, 200. https://doi.org/10.1007/s00604-019-3315-y (2019).
14. Cuhadar, S., Atay, A., Koseoglu, M., Dirican, A. & Hur, A. Stability studies of common biochemical analytes in serum separator tubes with or without gel barrier subjected to various storage conditions. *Biochem. Med. (Zagreb)*. **22** (2), 202–214. https://doi.org/10.11613/bm.2012.023 (2012).
15. Ehsan, M. A. et al. Fabrication of nanostructured Pd thin films using aerosol-assisted chemical vapor deposition for the nonenzymatic electrochemical detection of H_2O_2. *ACS Appl. Electron. Mater.* **1**, 417–429. https://doi.org/10.1021/acsaelm.8b00131 (2019).
16. Hasan, M. M. et al. Selective detection of dopamine at the AACVD synthesized palladium nanoparticles and Understanding the sensing mechanism through electrochemical and computational study. *J. Electrochem. Soc.* **166**, B1528–B1542. https://doi.org/10.1149/2.0631915jes (2019).
17. Ye, Q., Zhang, Z., Liu, J. & Wang, X. Screen-printed electrode-based biosensors modified with functional nucleic acid probes and their applications in this pandemic age: A review. *Anal. Methods*. **14**, 2961–2975. https://doi.org/10.1039/D2AY00666A (2022).
18. Ahammad, A. J. S. et al. Pyrolytic Preparation of gold nanoparticle-coated Taro carbon and its application for the selective detection of dopamine. *New. J. Chem.* **42**, 4543–4552. https://doi.org/10.1039/C7NJ04777K (2018).
19. Islam, T. et al. Fabrication of Ni–Co-based heterometallo-supramolecular polymer films and the study of electron transfer kinetics for the nonenzymatic electrochemical detection of nitrite. *ACS Appl. Polym. Mater.* **2**, 273–284. https://doi.org/10.1021/acsapm.9b00797 (2020).
20. Ahammad, A. J. S. et al. Porous Tal palm carbon nanosheets: preparation, characterization and application for the simultaneous determination of dopamine and uric acid. *Nanoscale Adv.* **1**, 613–626. https://doi.org/10.1039/c8na00090e (2019).
21. Staden, S. V. Nanostructured materials detect dopamine in biological fluids. *J. Electrochem. Soc.* **164**, B561–B566. https://doi.org/10.1149/2.1961712jes (2017).
22. Farzadnia, N., Bahmani, S. H., Asadi, A. & Hosseini, S. Mechanical and microstructural properties of cement pastes with rice husk Ash coated with carbon nanofibers using a natural polymer binder. *Constr. Build. Mater.* **175**, 691–704. https://doi.org/10.1016/j.conbuildmat.2018.04.205 (2018).
23. Li, Z., Li, Y. & Zhu, J. Straw-based activated carbon: optimization of the Preparation procedure and performance of volatile organic compounds adsorption. *Materials* **14**, 3284. https://doi.org/10.3390/ma14123284 (2021).
24. Zhang, H. et al. Biomass-derived carbon materials for electrochemical sensing: recent advances and future perspectives. *Crit. Rev. Anal. Chem.* 1–26. https://doi.org/10.1080/10408347.2024.2401504 (2024).
25. Haque, M. A. et al. Hollow reticular shaped highly ordered rice husk carbon for the simultaneous determination of dopamine and uric acid. *Electroanalysis* **32**, 1957–1970. https://doi.org/10.1002/elan.202060059 (2020).
26. Thai Rice Exporters Association. Rice Exports Statistics. Retrieved 27. from February (2025). http://www.thairiceexporters.or.th/statistic_2024.html (2024).
27. Onfray, C. & Thiam, A. Biomass-derived carbon-based electrodes for electrochemical sensing: A review. *Micromachines* **14**, 1688. https://doi.org/10.3390/mi14091688 (2023).
28. Kumar, V. G. et al. Rice straw derived cellulose nanofibers modified with L-histidine for ultra-trace fluorometric assay of Cr(VI) and Hg(II) in aqueous medium. *J. Clean. Prod.* **391**, 136106. https://doi.org/10.1016/j.jclepro.2023.136106 (2023).
29. Yang, W. et al. N/O co-doping porous biomass carbon constructed electrochemical sensor for universal and sensitive detection to Mycotoxins. *Food Chem.* **475**, 143397. https://doi.org/10.1016/j.foodchem.2025.143397 (2025).
30. Sun, Q. et al. Rice straw-derived carbon-based nanozyme sensor: application of identifying human urine Xanthine content and study of active sites. *Appl. Surf. Sci.* **602**, 154372. https://doi.org/10.1016/j.apsusc.2022.154372 (2022).
31. Sangon, S., Hunt, A. J., Ngernyen, Y., Youngme, S. & Supanchaiyamat, N. Rice straw-derived highly mesoporous carbon-zinc oxide nanocomposites as high-performance photocatalytic adsorbents for toxic dyes. *J. Clean. Prod.* **318**, 128583. https://doi.org/10.1016/j.jclepro.2021.128583 (2021).
32. Sangon, S. et al. $ZnCl_2$ activated mesoporous carbon from rice straw: optimization of its synthetic process and its application as a highly efficient adsorbent for amoxicillin. *Environ. Sci. : Water Res. Technol.* **10**, 1389. https://doi.org/10.1039/d4ew00171k (2024).
33. Łukaszewski, M., Soszko, M. & Czerwiński, A. Electrochemical methods of real surface area determination of noble metal Electrodes – an overview. *Int. J. Electrochem. Sci.* **11** (6), 4442–4469. https://doi.org/10.20964/2016.06.71 (2016).
34. Shao, M., Odell, J. H., Choi, S. I. & Xia, Y. Electrochemical surface area measurements of platinum- and palladium-based nanoparticles. *Electrochem. Commun.* **31**, 46–48. https://doi.org/10.1016/j.elecom.2013.03.011 (2013).
35. Thommes, M. et al. Physisorption of gases, with special reference to the evaluation of surface area and pore size distribution (IUPAC technical Report). *Pure Appl. Chem.* **87** (9-10), 1051–1069. https://doi.org/10.1515/pac-2014-1117 (2015).
36. Yang, J. & Qiu, K. Development of high surface area mesoporous activated carbons from herb residues. *Chem. Eng. J.* **167** (1), 148–154. https://doi.org/10.1016/j.cej.2010.12.013 (2011).
37. Ozdemir, I., Şahin, M., Orhan, R. & Erdem, M. Preparation and characterization of activated carbon from grape stalk by zinc chloride activation. *Fuel Process. Technol.* **125**, 200–206. https://doi.org/10.1016/j.fuproc.2014.04.002 (2014).
38. Yang, T. & Lua, A. C. Textural and chemical properties of zinc chloride activated carbons prepared from pistachio-nut shells. *Mater. Chem. Phys.* **100** (2–3), 438–444. https://doi.org/10.1016/j.matchemphys.2006.01.039 (2006).
39. Wu, W. et al. Chemical characterization of rice straw-derived Biochar for soil amendment. *Biomass Bioenergy*. **47**, 268–276. https://doi.org/10.1016/j.biombioe.2012.09.034 (2012).

40. Yang, J. et al. Low-temperature growth and optical properties of Ce-doped ZnO nanorods. *Appl. Surf. Sci.* **255** (5), 2646–2650. https://doi.org/10.1016/j.apsusc.2008.08.001 (2008).
41. Sharma, M. et al. ZnO tetrapods and activated carbon based hybrid composite: adsorbents for enhanced decontamination of hexavalent chromium from aqueous solution. *Chem. Eng. J.* **358**, 540–551. https://doi.org/10.1016/j.cej.2018.10.031 (2019).
42. Xu, J. et al. Effect of silver ions on the structure of ZnO and photocatalytic performance of Ag/ZnO composites. *Appl. Surf. Sci.* **255** (5), 1996–1999. https://doi.org/10.1016/j.apsusc.2008.06.130 (2008).
43. Ballerini, G., Ogle, K. & Barthés-Labrousse, M. G. The acid–base properties of the surface of native zinc oxide layers: an XPS study of adsorption of 1,2-diaminoethane. *Appl. Surf. Sci.* **253** (16), 6860–6867. https://doi.org/10.1016/j.apsusc.2007.01.126 (2007).
44. Shrotri, A., Kobayashi, H. & Fukuoka, A. Air oxidation of activated carbon to synthesize a biomimetic catalyst for hydrolysis of cellulose. *ChemSusChem* **9**, 1299–1303. https://doi.org/10.1002/cssc.201600279 (2016).
45. Tefera, M., Tessema, M., Admassie, S. & Wubet, W. Voltammetric determination of uric acid using multiwall carbon nanotubes coated-poly(4-amino-3-hydroxy naphthalene sulfonic acid) modified glassy carbon electrode. *Heliyon* **7**, e07575. https://doi.org/10.1016/j.heliyon.2021.e07575 (2021).
46. Gaya, E., Menendez, N., Mazario, E. & Herrasti, P. Fe_3O_4-Nanoparticle-Modified sensor for the detection of dopamine, uric acid and ascorbic acid. *Chemosensors* **11** (2), 79. https://doi.org/10.3390/chemosensors11020079 (2023).
47. Masrat, S. et al. Electrochemical ultrasensitive sensing of uric acid on Non-Enzymatic porous Cobalt oxide Nanosheets-Based sensor. *Biosensors* **12** (12), 1140. https://doi.org/10.3390/bios12121140 (2022).
48. Kadri, Y., Bekri-Abbess, I. & Herrasti, P. Highly sensitive Enzyme-free sensor based on a carbon paste electrode modified with binary zinc oxide/polyaniline nanocomposites for dopamine, ascorbic acid and uric acid sensing. *Electroanalysis* **35**, e202200248. https://doi.org/10.1002/elan.202200248 (2023).
49. Suratman, A. A., Zakaria, A. Z. C., Aziz, S. F. N. A. & Ahmad, S. A. A. Sensitive and selective non-enzymatic rGO/ZIF-8 hybrid composite-based electrochemical sensor for uric acid detection: optimisation by response surface methodology. *Microchem J.* **207**, 112214. https://doi.org/10.1016/j.microc.2024.112214 (2024).
50. Wangchuk, S. et al. A portable disposable metal-free electrochemical sensor for uric acid measurement in human blood serum. *Microchem J.* **207**, 112216. https://doi.org/10.1016/j.microc.2024.112216 (2024).
51. Nguyen, N. K. T. et al. A novel enzymeless electrochemical sensor based on $Ni(OH)_2$–NiO(OH) nanoelectrocatalyst for sensitive and selective detection of uric acid in PBS simulated body fluid. *Mater. Chem. Phys.* **327**, 129870. https://doi.org/10.1016/j.matchemphys.2024.129870 (2024).
52. Karim, A. et al. A review: progress and trend advantage of dopamine electrochemical sensor. *J. Electroanal. Chem.* **959**, 118157. https://doi.org/10.1016/j.jelechem.2024.118157 (2024).

Acknowledgements

This research project was financially supported by Mahasarakham University. We thank the Veterinary Research and Development Center (Upper Northern Region) Department of Livestock Development, Thailand. Partial support from Chiang Mai University and PERCH-CIC are acknowledged. We appreciate Chalida Phimsak and Sukanya Naeothaworn for their assistance in preparing research data.

Author contributions

P.N., J.L., T. K., and J.U. wrote the manuscript. P.N. interpreted the results. A.J.H., N.S., and S. S. performed the synthesis and characterizations of materials. J.J. provided the resources and revised the manuscript. J.U. designed the work, performed the experiments, interpreted the results, and revised the manuscript.

Declarations

Competing interests

The authors declare no competing interests.

Additional information

Supplementary Information The online version contains supplementary material available at https://doi.org/10.1038/s41598-025-03405-w.

Correspondence and requests for materials should be addressed to J.U.